Available online at www.sciencedirect.com
SCIENCE DIRECT®
International Journal of Heat and Fluid Flow 25 (2004) 785–794
International Journal of HEAT AND FLUID FLOW
www.elsevier.com/locate/ijhff

Assessment of realizability constraints in $\overline{v^2}$–f turbulence models

A. Sveningsson *, L. Davidson

Department of Mechanical Engineering, Division of Termo and Fluid dynamics, Chalmers University of Technology, 41296 Gothenburg, Sweden

Received 10 February 2004; accepted 12 May 2004
Available online 4 July 2004

Abstract

The use of the realizability constraint in $\overline{v^2}$–f turbulence models is assessed by computing a stator vane passage flow. In this flow the stagnation region is large and it is shown that the time scale bound suggested by [Int. J. Heat Fluid Flow 17 (1995) 89] is well suited to prevent unphysical growth of turbulence kinetic energy. However, this constraint causes numerical instabilities when used in the equation for the relaxation parameter, f. It is also shown that the standard use of the realizability constraint in the $\overline{v^2}$–f model is inconsistent and some modifications are suggested. These changes of the $\overline{v^2}$–f model are examined and shown to have negligible effect on the overall performance of the $\overline{v^2}$–f model. In this work two different versions of the $\overline{v^2}$–f model are investigated and the results obtained are compared with experimental data. The model on a form similar to that originally suggested by Durbin (e.g. [AIAA J. 33 (1995) 659]) produced the overall best agreement with stator vane heat transfer data.

Keywords: $\overline{v^2}$–f; Realizability constraint; Eddy viscosity

1. Introduction

During the last few years the $\overline{v^2}$–f turbulence model, originally suggested by Durbin (1991), has become increasingly popular due to its ability to correctly account for near-wall damping without use of so called damping functions. The reason why these, in many contexts questionable, damping functions can be avoided is the availability of an additional turbulent velocity scale—a generic wall normal Reynolds stress component, $\overline{v^2}$. By considering the exact transport equations for the Reynolds stresses in a fully developed channel flow it can readily be shown that the production of $\overline{uv}$ (the only Reynolds stress component that affects the mean flow field) should be proportional to $\overline{v^2}$. In two-equation models this velocity scale (squared) is not explicitly available but is replaced with the turbulence kinetic energy k. As k has a different wall distance dependency (y^2) than $\overline{v^2}$ (y^4) this modelling is expected to be inaccurate as walls are approached. This deficiency can to some extent be controlled by introducing a damping function that improves the wall distance dependence of $\overline{uv}$. Durbin (1991) showed that by simply replacing k with $\overline{v^2}$ in the definition of the eddy-viscosity results were substantially improved. Hence, an alternative interpretation, or definition, of the damping function, say f_μ, is that $\overline{v^2} = f_\mu k$. The main problem with a damping function is that there can be only one and that this function can be tuned to only a limited number of test cases. In $\overline{v^2}$–f models on the other hand, $\overline{v^2}$ is governed by a separate transport equation and thus has a potential of being applicable to a wider range of flow situations. One important feature of the $\overline{v^2}$ equation is its ability to account for non-local effects (e.g. kinematic blocking) by solving an elliptic relaxation equation for f, a parameter closely related to the pressure strain redistribution term. For an extensive discussion on this subject see Manceau et al. (2001).

The $\overline{v^2}$–f model has in many fluid flows where complex flow features are present shown to be superior to other RANS methods. For example, Parneix et al. (1998) successfully computed the strongly three-dimensional flow around a wall-mounted appendage. Using the $\overline{v^2}$–f model Hermanson et al. (2003) obtained improvements in predicted heat transfer rates as compared to k–ε computations for a stator vane flow. Similar results were also found in Sveningsson (2003).

* Corresponding author: Fax: +46-31-180976.
E-mail address: svening@tfd.chalmers.se (A. Sveningsson).

0142-727X/$ - see front matter © 2004 Elsevier Inc. All rights reserved.
doi:10.1016/j.ijheatfluidflow.2004.05.014

Nomenclature

C	vane chord; turbulence model constant
f_μ	damping function
f	relaxation variable, cf. Eq. (8)
H	stator vane height
h	heat transfer coefficient, $h = q_{\text{wall}}/(T_{\text{wall}} - T_{\text{in}})$
k	turbulent kinetic energy
L	turbulent length scale
P	vane pitch; mean pressure
p	pressure fluctuation
P_k	production term
Pr	Prandtl number
Pr_t	turbulent Prandtl number
S	$S^2 = S_{ij}S_{ij}$
S_{ij}	strain rate tensor
St	Stanton number, $St = h/\rho C_p U_{in}$
$\mathscr{T}$	turbulent time scale
U_i	mean velocities
u_i	velocity fluctuations
$\overline{v^2}$	turbulent velocity scale
$\overline{u_i u_j}$	Reynolds stresses
y	wall normal distance

Greeks

ε	dissipation rate of k
ν	kinematic viscosity
ν_t	eddy viscosity
ρ	density
$\sigma_k, \sigma_\varepsilon$	turbulence model constants

Superscript

+	variable normalized using wall parameters

Subscripts

in	inlet
w	wall value
∞	freestream value

Another class of flows where the $\overline{v^2}$–f model seems to work well is separated flows. Cokljat et al. (2003) computed a set of recirculating flows and found that the $\overline{v^2}$–f model in most cases outperformed two-equation approaches. The same trend was seen in Iaccarino (2001) where the flow in an asymmetric diffusor was computed using the $\overline{v^2}$–f model and the Launder–Sharma low-Reynolds number k–ε model. The separation bubble characteristic of this flow was fairly accurately predicted with the $\overline{v^2}$–f model whereas the k–ε model produced no recirculation at all.

Due to the somewhat unstable formulation of the wall boundary condition of the relaxation parameter, f, in the original formulation of the $\overline{v^2}$–f model Lien and Kalitzin (2001) slightly redefined f in order to have a numerically more attractive boundary condition. Due to the improved numerical properties of the redefined model it has become more popular than the original, which in most cases requires a coupled solution procedure (e.g. Sveningsson, 2003). In this study the behaviour of two versions of the $\overline{v^2}$–f model are compared in an attempt to investigate in what aspects they differ and also to improve the overall understanding of $\overline{v^2}$–f models' performance.

The test case used in this work is a linear cascade flow. Both two and three-dimensional computations are performed. Due to the strong blocking in this flow it is crucial to handle the overprediction of turbulent kinetic energy commonly encountered in stagnation point flows when linear eddy-viscosity based models are used for turbulence closure. This deficiency is here handled by use of a realizability constraint written in terms of an upper time scale bound as proposed by Durbin (1995a). In general the realizability constraint is somewhat more sophisticated (e.g. Lumley, 1978) but throughout this paper the realizability constraint refers to a bound on the turbulence time (or length) scale derived from the requirement that no turbulence energy component may be negative. As a matter of fact the $\overline{v^2}$–f model is almost always used in conjunction with this time scale bound and the central part of this work is an investigation of this combination. The reason for this investigation is that the time scale bound in quite a few cases causes computations to diverge. In later sections it will be shown that excluding it improves both the physics and the stability of the $\overline{v^2}$–f model and to what extent these changes affect the overall performance of the model is examined.

2. Governing equations

The governing equations are the Reynolds averaged Navier–Stokes (RANS) equations and equations for conservation of mass and energy. For an incompressible fluid the time averaged versions of these equations read

$$U_j \frac{\partial U_i}{\partial x_j} = -\frac{1}{\rho}\frac{\partial P}{\partial x_i} + \nu \frac{\partial^2 U_i}{\partial x_j^2} - \frac{\partial}{\partial x_j}\overline{u_i u_j}, \quad \frac{\partial U_j}{\partial x_j} = 0 \tag{1}$$

$$U_i \frac{\partial T}{\partial x_i} = \frac{\partial}{\partial x_i}\left(\frac{\nu}{Pr}\frac{\partial T}{\partial x_i} - \overline{u_i t}\right) \tag{2}$$

The unknown Reynolds stresses and the turbulent heat fluxes are closed using the eddy-viscosity concept, i.e.

Table 1
$\overline{v^2}$–f model constants

Model	C_μ	$C_{\varepsilon d}$	$C_{\varepsilon 2}$	C_1	C_2	σ_k	σ_ε	C_L	C_η
1: Parneix et al. (1998)	0.22	0.045	1.9	1.4	0.3	1.0	1.3	0.25	85
2: Kalitzin (1999)	0.19	0.045	1.9	0.4	0.3	1.0	1.3	0.23	70
2: Lien and Kalitzin (2001)	0.22	0.05	1.9	0.4	0.3	1.0	1.3	0.23	70
2: Cokljat et al. (2003)	0.22	0.045	1.9	0.4	0.3	1.0	1.3	0.23	70

$$\overline{u_i u_j} = -2\nu_t S_{ij} + \frac{2}{3}k\delta_{ij}; \quad \overline{u_i t} = -\frac{\nu_t}{Pr_t}\frac{\partial T}{\partial x_i} \tag{3}$$

$$\nu_t = C_\mu \overline{v^2}\mathscr{T}, \quad \text{where } \mathscr{T} = \max\left(\frac{k}{\varepsilon}, 6\sqrt{\frac{\nu}{\varepsilon}}\right) \tag{4}$$

A turbulence Prandtl number of 0.89 was used in computations that included heat transfer. The turbulent quantities k and ε are obtained by solving two additional transport equations that read

$$u_j\frac{\partial k}{\partial x_j} = \frac{\partial}{\partial x_j}\left(\left(\nu + \frac{\nu_t}{\sigma_k}\right)\frac{\partial k}{\partial x_j}\right) + P_k - \varepsilon \tag{5}$$

$$u_j\frac{\partial \varepsilon}{\partial x_j} = \frac{\partial}{\partial x_j}\left(\left(\nu + \frac{\nu_t}{\sigma_\varepsilon}\right)\frac{\partial \varepsilon}{\partial x_j}\right) + \frac{C_{\varepsilon 1}P_k - C_{\varepsilon 2}\varepsilon}{\mathscr{T}} \tag{6}$$

In the present study the performance of two different $\overline{v^2}$–f models have been compared. They will hereafter be referred to as model 1 and model 2, respectively. In model 1, given in Parneix et al. (1998), the wall-normal Reynolds stress component, $\overline{v^2}$, is modelled using

$$u_j\frac{\partial \overline{v^2}}{\partial x_j} = \frac{\partial}{\partial x_j}\left(\left(\nu + \frac{\nu_t}{\sigma_k}\right)\frac{\partial \overline{v^2}}{\partial x_j}\right) + kf - \frac{\overline{v^2}}{k}\varepsilon \tag{7}$$

$$L^2\frac{\partial^2 f}{\partial x_j^2} - f = \frac{C_1 - 1}{\mathscr{T}}\left(\frac{\overline{v^2}}{k} - \frac{2}{3}\right) - C_2\frac{P_k}{k} \tag{8}$$

The turbulent length scale, L, and the modified coefficient $C_{\varepsilon 1}$ are calculated using

$$L = C_L \max\left(\frac{k^{3/2}}{\varepsilon}, C_\eta\frac{\nu^{3/4}}{\varepsilon^{1/4}}\right), \quad C_{\varepsilon 1} = 1.4\left(1 + C_{\varepsilon d}\sqrt{k/\overline{v^2}}\right) \tag{9}$$

Unfortunately, the wall boundary conditions for the dissipation rate, ε, and the redistribution parameter, f,

$$\varepsilon \to 2\nu\left(\frac{k}{y^2}\right); \quad f \to \frac{-20\nu^2}{\varepsilon}\left(\frac{\overline{v^2}}{y^4}\right) \quad \text{as } y \to 0 \tag{10}$$

make the original formulation somewhat unstable. A modification to model 1 used in e.g. Kalitzin (1999) and Lien and Kalitzin (2001) solves this problem and renders the following $\overline{v^2}$ and f equations (model 2)

$$u_j\frac{\partial \overline{v^2}}{\partial x_j} = \frac{\partial}{\partial x_j}\left(\left(\nu + \frac{\nu_t}{\sigma_k}\right)\frac{\partial \overline{v^2}}{\partial x_j}\right) + kf - 6\overline{v^2}\frac{\varepsilon}{k} \tag{11}$$

$$L^2\frac{\partial^2 f}{\partial x_j^2} - f = \frac{C_1}{\mathscr{T}}\left(\frac{\overline{v^2}}{k} - \frac{2}{3}\right) - C_2\frac{P_k}{k} - 5\frac{\overline{v^2}}{k\mathscr{T}} \tag{12}$$

now with a homogeneous f wall boundary condition. Note that the models given in Lien and Kalitzin (2001) and Kalitzin (1999) only differ in model constant values. In Cokljat et al. (2003) yet another set of constants was used. All suggested values are listed in Table 1 and later the different sets of constants will be examined in a stator vane heat transfer computation.

2.1. The realizability constraint

Most eddy-viscosity based turbulence models over-predict the turbulent kinetic energy, k, in stagnation point flows. Durbin (1995a) suggested a bound on the turbulent time scale, $\mathscr{T}$, derived from $2k \geqslant \overline{u^2} \geqslant 0$, which significantly improves predictions of k. For $\overline{v^2}$–f models this constraint implies

$$\mathscr{T} = \min\left(\max\left(\frac{k}{\varepsilon}, 6\sqrt{\frac{\nu}{\varepsilon}}\right), \frac{C_{\lim}k}{3C_\mu\overline{v^2}}\frac{1}{\max\lambda_\alpha}\right) \tag{13}$$

where the constant $C_{\lim}$ has been added to allow for tuning against experiments and $\max\lambda_\alpha$ is the largest eigenvalue of the strain rate tensor S_{ij}. In three dimensions $|\lambda_\alpha| \leqslant (2S/3)^{1/2}$ (in 2-D $|\lambda_\alpha| = (S/2)^{1/2}$), which can be used to obtain

$$\mathscr{T} = \min\left(\max\left(\frac{k}{\varepsilon}, 6\sqrt{\frac{\nu}{\varepsilon}}\right), \frac{C_{\lim}k}{6^{1/2}C_\mu\overline{v^2}S}\right) \tag{14}$$

Now, let us return to the k and ε equations in order to find out what mechanism is responsible for the improvement in the predicted levels of the turbulence kinetic energy. It has been argued that it is the use of the realizability constraint in the ε equation that is the key as it increases the production term, $P_\varepsilon = C_{\varepsilon 1}P_k/\mathscr{T}$ (lower $\mathscr{T}$ higher P_ε). If we write the ε source terms on another form we see that this is not the case

$$\frac{C_{\varepsilon 1}2\nu_t S_{ij}S_{ij} - C_{\varepsilon 2}\varepsilon}{\mathscr{T}} = 2C_{\varepsilon 1}C_\mu\overline{v^2}S_{ij}S_{ij} - \frac{C_{\varepsilon 2}\varepsilon}{\mathscr{T}} \tag{15}$$

where $P_k = 2\nu_t S_{ij}S_{ij}$ and Eq. (4) for the eddy viscosity have been used. Clearly the effect a limitation of the time scale has in the ε equation is not to increase the production of ε but to increase its dissipation. The increase in dissipation of ε will lower the level of ε, i.e. decrease

the dissipation rate of k, and thus lead to *higher* levels of k. If the explanation cannot be found in the ε equation it must come from the k equation, where the only term involving $\mathscr{T}$ is P_k. Hence, the mechanism responsible for the improvement in k is the reduction in modelled production rate, i.e.

$$P_k = 2C_\mu \overline{v^2}\mathscr{T} S_{ij}S_{ij} \tag{16}$$

which to some extent is reduced by the modification of the time scale in the ε equation.

2.2. On the use of realizability constraints in the $\overline{v^2}$–f model

In order to illustrate the effect of realizability rewrite the f equation (Eq. (12)) as

$$0 = \frac{C_2 P_k}{L^2 k} + \frac{1}{\mathscr{T} L^2}\left[(5 - C_1)\frac{\overline{v^2}}{k} + \frac{2}{3}C_1\right] - \frac{f}{L^2} + \frac{\partial^2 f}{\partial x_j^2} \tag{17}$$

The first two terms are source terms ($C_1 = 0.4$), the third act as a sink whereas the last term is a diffusive term. Now imagine our time scale limiter being active. This means that P_k/k in the first source term initially will decrease (as P_k will affect k it is not obvious whether the quantity P_k/k at a later stage will actually decrease or increase). This decrease will to some extent be balanced by an increase of the second source term as this term is multiplied by $1/\mathscr{T}$. Since the objective of the limit of $\mathscr{T}$ is to reduce k (and ν_t) this countereffect is incorrect as kf is the source term in the $\overline{v^2}$ equation.

From inspection of Eq. (14), we see that an increase of $\overline{v^2}$ further reduces the time scale $\mathscr{T}$. This positive feedback often caused the stator vane computations to diverge as f became increasingly larger. Note that the f equation is of elliptic nature and that any perturbation is felt in the entire computational domain. The easiest way to get around this problem is to not use the time scale limit at all in the f equation. Another possible route is to rewrite the realizability constraint in terms of $\overline{v^2}/k$, i.e.

$$\frac{\overline{v^2}}{k} = \min\left[\frac{\overline{v^2}}{k}, \frac{C_{\lim}}{\sqrt{6}C_\mu \mathscr{T} S}, 2\right] \tag{18}$$

Using this limit in the f equation will consistently lower the $\overline{v^2}$ part of the turbulence kinetic energy.

Finally, Lien and Kalitzin (2001) suggested a similar bound on the turbulent length scale L appearing in the f equation, which has also been investigated

$$L = C_{\mathrm{L}} \max\left(\min\left(\frac{k^{3/2}}{\varepsilon}, \frac{k^{3/2}}{\sqrt{6}C_\mu \overline{v^2} S}\right), C_\eta \frac{\nu^{3/4}}{\varepsilon^{1/4}}\right) \tag{19}$$

2.2.1. The consequence of realizability in the farfield

In the farfield the elliptic operator $\partial^2 f/\partial x_j^2$ is assumed to be negligible (in fact, Davidson et al. (2003) showed that this is not the case even for fully developed channel flow) and the f equation of model 2 reduces to

$$-f = \frac{C_1}{\mathscr{T}}\left(\frac{\overline{v^2}}{k} - \frac{2}{3}\right) - C_2\frac{P_k}{k} - 5\frac{\overline{v^2}}{k\mathscr{T}} \tag{20}$$

With this expression for f the $\overline{v^2}$ equation source term in Eq. (11) becomes

$$-\frac{C_1}{\mathscr{T}}\left(\overline{v^2} - \frac{2}{3}k\right) + C_2 P_k + 5\frac{\overline{v^2}}{\mathscr{T}} - 6\frac{\overline{v^2}}{k}\varepsilon \tag{21}$$

Now assume we have an isotropic flow ($\overline{v^2} = 2k/3$), in which the production of k is negligible. We get

$$+\frac{10k}{3\mathscr{T}} - \frac{12}{3}\varepsilon \tag{22}$$

which yields the correct isotropic dissipation rate $-2\varepsilon/3$ when $\mathscr{T} = k/\varepsilon$. But when the flow approaches a stagnation region the value of $\mathscr{T}$ becomes smaller than k/ε (or $\varepsilon < k/\mathscr{T}$) as the time scale bound is activated (cf. Fig. 5(a)). As already mentioned the time scale bound ought to decrease $\overline{v^2}$ but clearly, from Eq. (22), it will cause a physically incorrect production of $\overline{v^2}$. This production increases $\overline{v^2}$, which further restrains the time scale bound (Eq. (14)) and we might again end up with numerical problems due to positive feedback. Note that this inconsistency is not present in model 1. The obvious solution to this anomaly is to not use the realizability constraint in the f equation or to change the modelled $\overline{v^2}$ dissipation rate (model 2) according to

$$\varepsilon_{\overline{v^2}} = -5\frac{\overline{v^2}}{\mathscr{T}} - \frac{\overline{v^2}}{k}\varepsilon \tag{23}$$

One of these modifications proved to be necessary in order to achieve a converged solution with model 2 for the stator vane computations where the stagnation region indeed is very large.

3. Solver

CALC-BFC (boundary fitted coordinates) is a structured finite volume code using the pressure correction scheme SIMPLEC and a co-located grid arrangement with Rhie and Chow interpolation. The van Leer scheme (a bounded, second order upwind scheme) was used when discretizising the momentum turbulence and energy equations. Due to convergence problems false time stepping was used to enhance numerical stability. The momentum equations were solved with a segregated tri-diagonal matrix solver (TDMA) and the turbulence equations were solved with either a segregated (model 2) or coupled (model 1) TDMA (for details see Sveningsson (2003)). All fluid properties were treated as being constant.

4. Results

4.1. The effect of the realizability constraint in a stagnation point flow

In order to illustrate the importance of the realizability constraint some two-dimensional computations of a stator vane flow were conducted. The vane profile, shown in Fig. 1 together with the computational domain, is the same as the vane experimentally investigated in, e.g., Radomsky and Thole (2000). The rig is a scaled-up linear cascade with vanes of chord length $C = 0.594$ m. The inlet turbulence intensity of the flow is $\mathrm{Tu}_{\mathrm{in}} = 0.6\%$ and a measured turbulent length scale was used to obtain an inlet ε boundary condition.

In Fig. 2 contours of k/U_{in}^2 for the stator vane flow are shown. In all three cases $\overline{v^2}$–f model 1 has been used with the only difference that in Fig. 2(a) the realizability constraint, Eq. (14), is deactivated, in Fig. 2(b) the constraint is used when calculating ν_{t} and in the ε equation, whereas in Fig. 2(c) it has been used everywhere the time scale $\mathscr{T}$ appears. It can be seen that the constraint has a strong influence. For example, when the limiter is active it is only in a narrow region around the wake that k/U_{in}^2 exceeds levels of 10^{-3}, whereas the same quantity is well above this value in almost the entire domain if the constraint is not used.

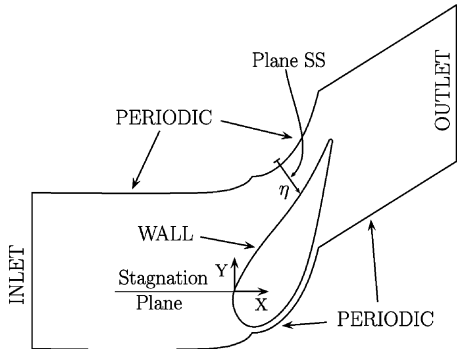

Fig. 1. Computational domain together with the locations of the stagnation plane and plane SS, which are used when post-processing the results of the three-dimensional computations. Whenever the coordinate η is used $\eta = 0$ is located on the suction side wall, whereas $\eta = 1$ lies on the pressure side of the vane.

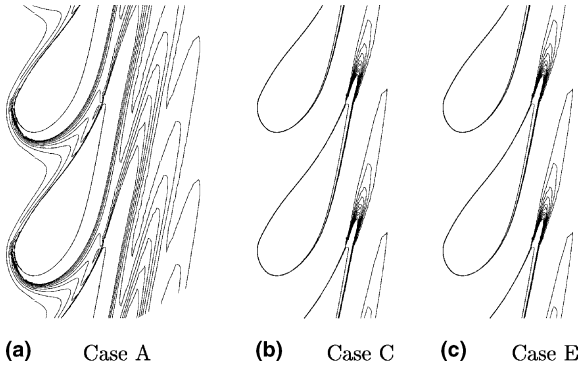

Fig. 2. Contours of k/U_{in}^2. Inlet flow from left. Contour intervals of 0.001. Description of Cases A, C and E are given in Table 2.

In Section 2.1 the effects of an upper bound on the turbulent time scale, $\mathscr{T}$, in different terms in the governing equations were discussed. The conclusions drawn in that section will now be examined in detail. First of all, as Fig. 2(a) and (b) show drastically different results, it must be the use of the time scale bound in the expression for ν_{t} (or possibly in the ε equation) that prevents the turbulent kinetic energy from taking erroneous values. Use of the bound also in the f equation has little effect on the k distribution as Fig. 2(b) and (c) are very similar. In order to make a quantitative comparison of the effect realizability has on the k distribution k/U_{in}^2 is plotted along the stagnation line in Fig. 3. All these computations are carried out using model 1 and in each case the time scale bound is used as given in Table 2.

In Fig. 3(a) the importance of using the time scale bound is again obvious. The k profile obtained without the bound has a maximum about 30 times higher than the maximum of any other profile. The influence of C_{lim} is also illustrated. In the close-up (Fig. 3(b)) it can be

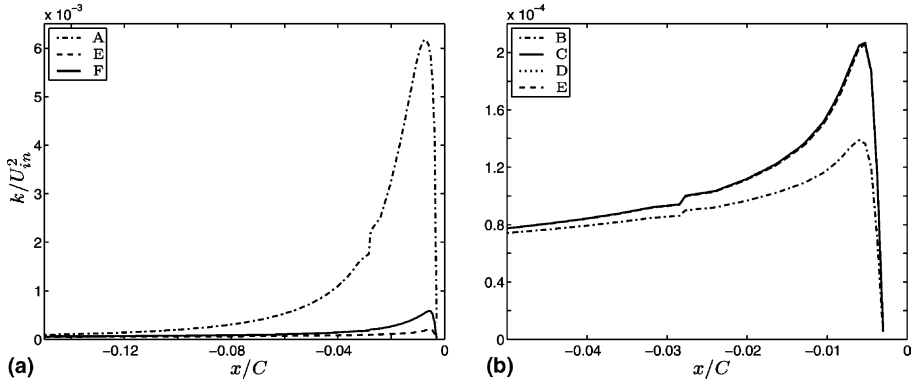

Fig. 3. Profiles of k/U_{in}^2 approaching the stagnation point for different realizability constraints. For legend see Table 2. (a) Global view; (b) Close-up.

Table 2
Description of how realizability is used when investigating its influence in the stagnation region

Case	Description
A	No realizability constraint (RC)
B	RC on $\mathscr{T}$ used in ν_t ($C_{lim} = 0.6$)
C	RC on $\mathscr{T}$ used in ν_t and ε equation
D	RC on $\mathscr{T}$ used in ν_t, ε and f equations
E	RC on $\mathscr{T}$ and L used in ν_t, ε and f equations
F	Same as E but with $C_{lim} = 1.0$

seen that the use of the realizability constraint (in terms of $\mathscr{T}$, or L) in the f equation has only a limited influence on k. The profile that deviates from the other is the one where the time scale bound has only been used in the ν_t expression (recall that this was the expected effect discussed in the previous section). Hence, it can be concluded that the use of the bound in the f equation is not important, that using it in the ε equation *increases* k (i.e. k is lower without the bound, cf. Fig. 3(b)) and that the only reason that the constraint works is the limitation of the turbulent viscosity.

For the $\overline{v^2}$ profiles along the stagnation line the differences are somewhat larger. In Fig. 4(a) profiles of the normalized wall normal Reynolds stress component, $\overline{v^2}/U_{in}^2$, are shown. We see that Case B, consistent with the lower values of k in Fig. 3(b), gives lower values than Cases C and E. Also of interest is that Case D gives the same results as Case E (not shown in Fig. 4(a) as the curves overlap), which is a surprise as the corresponding bound on $\mathscr{T}$ had such a strong impact on the turbulence field. This can only be explained by the fact that the expression for the turbulent length scale (Eq. (19)) is unaffected by the realizability constraint. Clearly, from Eq. (19), this can only be the case if the *lower* bound on L, expressed in Kolmogorov variables, is always greater than $k^{3/2}/\varepsilon$. Obviously, this also means that the order in which the two limits in this expression are executed is of importance. The present procedure is to first check whether the normal components of the Reynolds stress tensor is always positive (the realizability constraint), whereafter the resulting quantity is compared with the "viscous" length scale. In Fig. 5(b) contours of the ratio of the viscous and the turbulent length scales are plotted. It can be seen that the viscous length scale ($C_\eta \nu^{3/4}/\varepsilon^{1/4}$) is many times larger than the turbulent length scale ($k^{3/2}/\varepsilon$) in the entire domain. This means that if the procedure would be reversed, as is the case

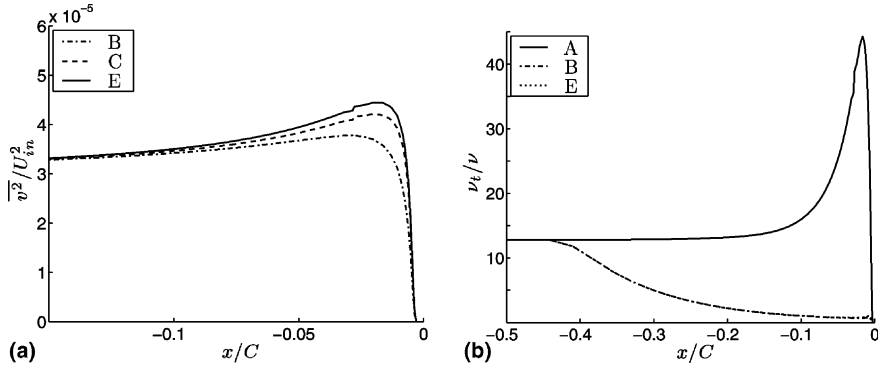

Fig. 4. Profiles of $\overline{v^2}/U_{in}^2$ (a) and ν_t/ν (b) approaching the stagnation point for different realizability constraints. For legend see Table 2.

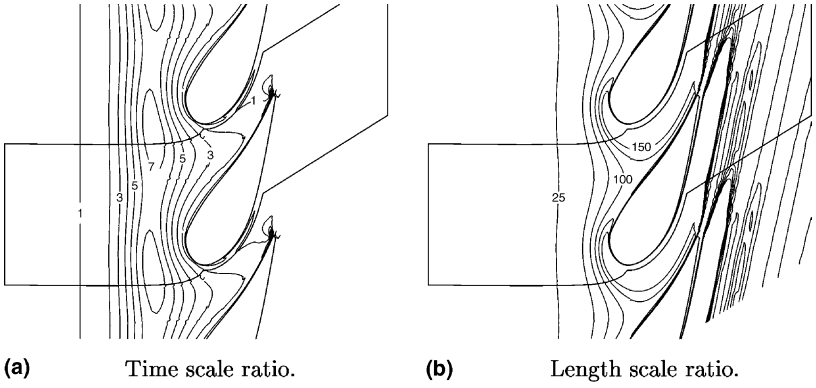

Fig. 5. (a) Contours of $(k/\varepsilon)/\mathscr{T}$ at midspan indicating in which areas the time scale constraint is active. For values above 1 the constraint is active; (b) Contours of $(C_\eta \nu^{3/4}/\varepsilon^{1/4})/(k^{3/2}/\varepsilon)$ indicating in which areas the viscous length scale in Eq. (19) is active.

when the time scale limits are executed, the length scale derived from the realizability constraint would dominate the field. Note that the results shown in Fig. 5 are from a low turbulence intensity computation ($Tu_{in} = 0.6\%$). For the high turbulence intensity case ($Tu_{in} = 10\%$) the length scale ratio behaved as expected, i.e. the viscous length scale was only active in a near-wall region around the vane.

Finally, the influence of the realizability constraint on the turbulent viscosity, ν_t, is illustrated in Fig. 4(b), where the normalized turbulent viscosity ν_t/ν along the stagnation line is plotted. Just as for the other turbulent quantities the constraint has a remarkable effect on ν_t. As soon as the presence of the vane makes the flow decelerate (or accelerate) the eigenvalues of the strain rate tensor, S_{ij}, becomes large enough to activate the time scale constraint (cf. Eq. (14)). In Fig. 5(a) contours of the ratio $(k/\varepsilon)/\mathscr{T}$ are shown. They indicate in which regions the time scale constraint is active and to what extent the turbulence time scale is modified. Wherever the ratio is greater than unity, which it is in almost the entire vane passage, the realizability constraint is active. This means that the turbulence model is modified in most of the domain. For example, the eddy viscosity in the active regions is given by $\nu_t = C_{lim}k/(3\max\lambda_\alpha)$, which is very different from the original ν_t expression. This suggests that the choice of the constant C_{lim} becomes rather important in stagnation point flows and that the original ν_t expression severely overestimates the eddy viscosity. Note that the physically justified lowest value of C_{lim} is unity, whereas a value of 0.6 has been used in Fig. 5(a). As the active region is large the lower value might cause too a strong bound on the turbulence time scale.

Also worth mentioning is that the minor difference between the results for Cases C and D indicates that the terms in the f equation involving $\mathscr{T}$, i.e. the so called slow terms, have only a limited influence on f; they are most often small compared to the rapid term, C_2P_k/k. Another issue of this work that seems to be related to this, is the overall stability of the $\overline{v^2}$–f model. When the f residuals of a non-converging computation were plotted the largest residuals were found in regions where large gradients in f coincided with regions of low turbulence production rate (P_k). Further, the $\overline{v^2}$–f model has been found to become numerically stiff for y^+ values below unity. Here too P_k is very small due to small values of ν_t. These observations suggest that it is when the slow terms dominate the f equation that the $\overline{v^2}$–f model becomes unstable.

4.1.1. The effect on vane heat transfer

In stator vane applications the predicted turbulence field is in most cases of secondary interest. Of greater concern is the rate of which heat is being transferred from the hot gas accelerating through the vane passage to the stator vane walls. However, in order to obtain a sufficiently accurate prediction of the heat transfer process (the turbulent heat fluxes) a fairly accurate prediction of the turbulence field is most often necessary. With the large impact of the realizability constraint on the turbulence field seen in the preceding section in mind we will in this section consider its effect on stator vane heat transfer. The performance of the two different versions of the $\overline{v^2}$–f model are also investigated and compared with measurements. In Fig. 6(a) the predicted stator vane Stanton number distributions are plotted together with measurements for some $\overline{v^2}$–f model 1 computations (Cases A–F, cf. Table 2). The inlet turbulence intensity is $Tu_{in} = 0.6\%$. s is a coordinate along the stator vane, $s/C < 0$ being the pressure side of the vane, whereas $s/C > 0$ corresponds to the suction side. In Fig. 6(b) the versions of the $\overline{v^2}$–f model given in Section 2 are compared for a case with higher turbulence intensity ($Tu_{in} = 10\%$). From both figures it can be seen that model 1 (solid lines) does exceptionally well in the region around the stagnation point ($s/C = 0$) and along the pressure side of the vane for both high and low

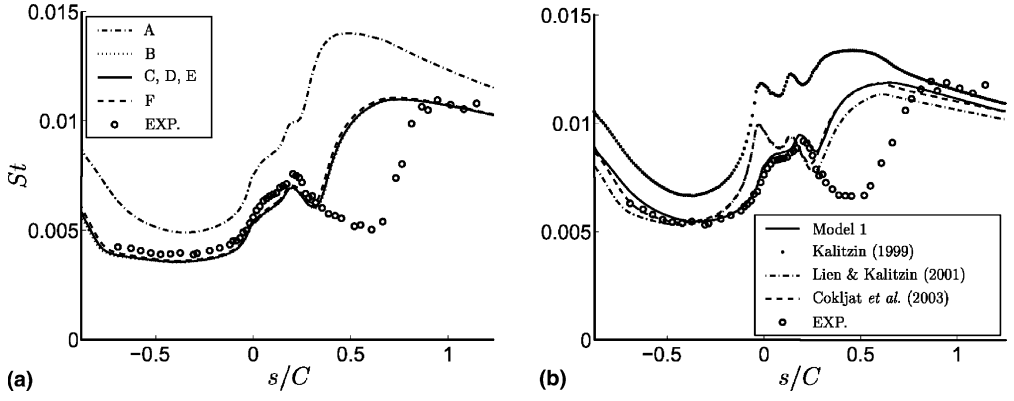

Fig. 6. Stator vane Stanton number. (a) Different realizability constraints using $\overline{v^2}$–f model 1. $Tu_{in} = 0.6\%$. For legend see Table 2; (b) Different $\overline{v^2}$–f models with different model constants (cf. Table 1). $Tu_{in} = 10\%$. $s/C > 0$ suction side, $s/C < 0$ pressure side.

turbulence intensity. On the suction side transition is predicted far too early, which has a strong impact on the heat transfer on the suction side. This feature is apparent in all computations and is only weakly dependent on the use of the realizability constraint.

From Fig. 6(a) we see that the predicted Stanton number increases by some 30–50% if the realizability constraint is deactivated. Also evident is that all the other cases produce almost identical Stanton number distributions, which supports the finding in previous sections, i.e. that the time scale bound is only important in the expression for the eddy viscosity. Somewhat surprisingly the change of the $C_{\lim}$ constant from 0.6 to 1.0 (Case F) has very little effect on the heat transfer.

The comparison of the different models in Fig. 6(b) reveals that the set of constants used in Kalitzin (1999) (model 2) is inappropriate, at least for heat transfer computations, giving values about 30% too high. We also see that the sets of constants used in Lien and Kalitzin (2001) and Cokljat et al. (2003) (both model 2) give similar results but do not reproduce the trend in the stagnation region as accurately as model 1 does. Both versions predict a peak in heat transfer right at the stagnation point whereas the measured peak lies some distance downstream this point.

4.2. The 3D stator vane flow

The main aim of this section is to investigate what a suitable value of the model constant $C_{\lim}$ might be. The test case is the three-dimensional flow in a stator vane passage investigated in, e.g. Radomsky and Thole (2000). For an extended discussion of the predicted three-dimensional flow field and the heat transfer to the plate on which the vanes are mounted the reader is referred to Sveningsson and Davidson (2004). All results in this section will be presented as either contour or vector plots in two different planes, the stagnation plane and plane SS, both shown in Fig. 1. Plane SS, cuts through the vane passage at about half a chord length into the passage (this plane is defined to be normal to the vane suction surface at a distance $s/C = 0.35$ from the stagnation point, s being a coordinate along the surface of the stator vane). Included in this figure is the definition of the coordinate η associated with plane SS. η ranges from 0 to 1, $\eta = 0$ being the suction side and $\eta = 1$ the pressure side.

In Fig. 7 contours of k/U_{in}^2 are plotted in the stagnation plane for different values of $C_{\lim}$. The results are in line with the conclusions drawn earlier. $C_{\lim} = \infty$ (no realizability constraint) gives too high production of k but when $C_{\lim}$ is reduced to 0.6 the region of high k associated with the stagnation point anomaly disappears. The region of large k associated with the roll-up of the horseshoe vortex on the other hand remains almost unaffected by the reduction of $C_{\lim}$. Also included

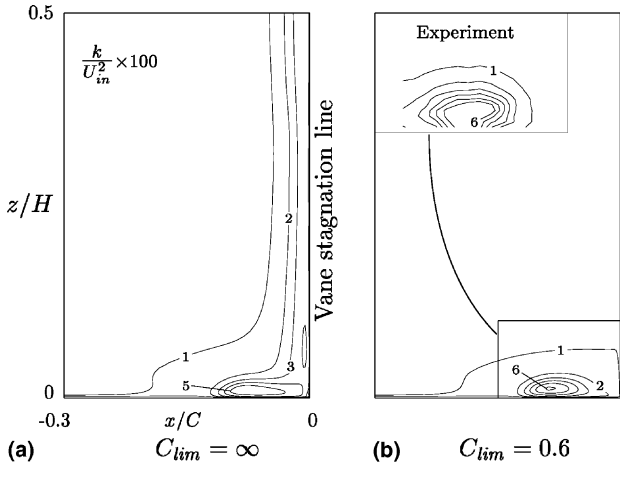

Fig. 7. Contours of normalized turbulent kinetic energy, k/U_{in}^2, in the stagnation plane for $\overline{v^2}$–f model 1 computations with and without the realizability constraint. Contour intervals of $0.01k/U_{\text{in}}^2$.

in Fig. 7(b) are contours of the corresponding measured quantity in a close-up of the lower right hand corner. It can be seen that the prediction (with use of realizability constraint) agrees well, both qualitatively and quantitatively, with the experimental data. By comparing Fig. 7(a) and (b) one would expect a weaker secondary motion (horseshoe vortex roll-up) in the former computation, especially downstream the leading edge region, as the values of k (and v_{t}) is high along the vane stagnation line. We will therefore examine the flow and turbulence field in plane SS (cf. Fig. 1) located some distance into the vane passage, where additional experimental data are available for comparison.

The effect of the realizability constraint on the turbulent kinetic energy in plane SS is shown in Fig. 8, where the k distribution normalized with the inlet velocity is given for some values of $C_{\lim}$. Again it is obvious that the choice of $C_{\lim}$ is important in $\overline{v^2}$–f models and that the model's improved physical foundation compared to two-equation models does not solve the problem of the stagnation point anomaly. In the contour plot second from the left, where the constraint is not used, the levels of k/U_{in}^2 are greater than 6% in a large portion of the plane with the exception of a region to the right where k/U_{in}^2 is slightly lower ($\approx 4.0\%$). Setting the value of $C_{\lim}$ to 1.0, i.e. using the time scale bound that can be algebraically derived, improves the prediction a great deal. Further reducing the value of $C_{\lim}$ to 0.6 gives peak values of $k/U_{\text{in}}^2 \approx 6.0\%$ at the center of the horseshoe vortices, which is in close agreement with the values found in experiments.

It is interesting that even if k is very sensitive to the choice of the model constant $C_{\lim}$ the value of 0.6 does give fairly accurate predictions of k in the stator vane test case of this study. This value has not been tuned to fit this particular set of experimental data but can be

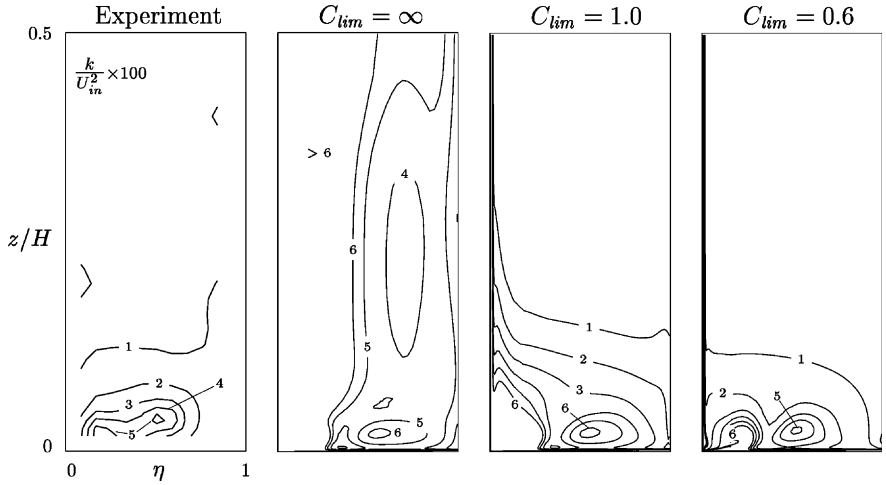

Fig. 8. Measured and predicted levels of normalized turbulence kinetic energy, k/U_{in}^2, in plane SS (cf. Fig. 1). Comparison of experimental data and three computations with different values of C_{lim}. Contour intervals of 1%. For reference, the freestream velocity at this location is approximately five times higher than at the inlet.

found in several investigations by other researches, e.g. Lien and Kalitzin (2001), Kalitzin (1999), which suggests that this value has a potential of being applicable to a wider range of flows.

With the very different k distributions in plane SS in mind we next turn to the influence of the realizability constraint on the secondary velocity field in the vane passage. As the eddy viscosity will be substantially overpredicted without the constraint we would expect a less intense secondary flow field when the time scale bound is deactivated. In this context the term "secondary flow" refers to structures like the pressure and suction side legs of the horseshoe vortex that sweep around the vane creating the characteristic horseshoe-like signature.

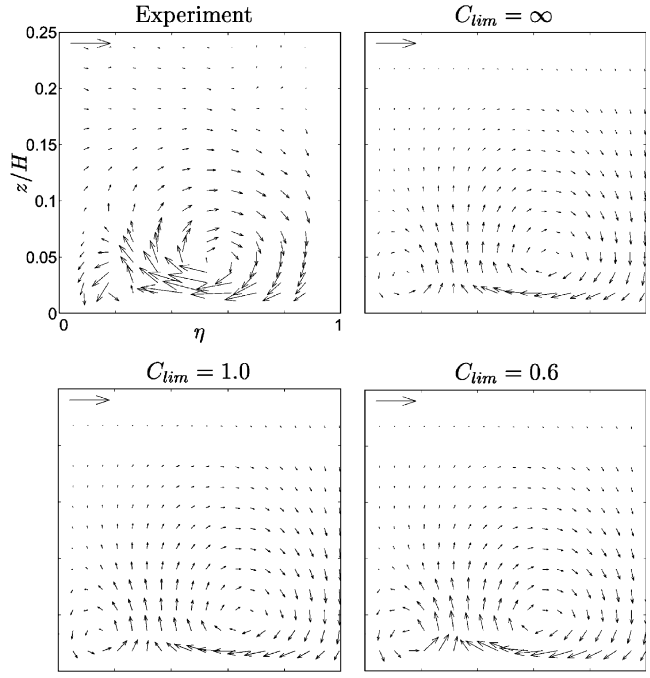

Fig. 9. Secondary velocities in the lower half of plane SS (cf. Fig. 1). Endwall located at $z = 0$. Suction and pressure surfaces located at $\eta = 0$ and 1, respectively. The reference arrows correspond to 20% of the maximum total velocity in the plane.

In Fig. 9 the secondary velocities defined in Kang and Thole (2000) for different values of C_{lim} are compared with experimental data. $\overline{v^2}$–f model 1 was used in all computations. First, it can be seen that the intensity of the secondary motion is underpredicted, especially the net flow from the pressure side towards the suction side of the vane. In Sveningsson (2003) it was shown that several commonly used two-equation models produced even weaker secondary motion and that the intensity of the secondary motion in the vane passage is largely determined by how well the flow in the stagnation region is captured. Second, the results indicate that the secondary velocities are not that sensitive to the realizability constraint. However, as expected, the secondary motion is somewhat weakened due to the extra viscosity produced when the realizability constraint is turned off.

5. Conclusions

The use of the realizability constraint in $\overline{v^2}$–f turbulence models has been assessed by computing a stator vane flow. In this flow the stagnation region is large and it was found that the constraint was necessary when calculating the eddy viscosity in order to prevent unphysical growth of turbulence kinetic energy. The mechanism responsible for the improvement is the reduction in production of turbulence kinetic energy. The constraint, expressed as an upper bound on the turbulent time scale, was found to cause numerical

instabilities when used in the f equation. It was also shown that the standard use of the realizability constraint in the $\overline{v^2}$–f model is inconsistent and some modifications were suggested. These changes of the $\overline{v^2}$–f model were carefully examined and were found to have negligible effect on the overall performance of the model. Therefore it is suggested that the turbulent time scale bound should be used only when calculating the eddy viscosity. In other words it is sufficient to use the realizability constraint ($\overline{u_\alpha^2} > 0$) to derive a bound on the eddy-viscosity itself, not the turbulent time scale. This bound would have the form

$$\nu_t = \min\left[\nu_t, \frac{C_{\lim} k}{6^{1/2} S}\right] \tag{24}$$

The corresponding bound on the turbulence length scale had in the present study no effect at all. This is due to the fact that the upper bound on the length scale, expressed in Kolmogorov variables, dominates in almost the entire computational domain.

Finally, the performance of two different versions of the $\overline{v^2}$–f models were investigated and the results were compared with experimental data. It was found that the model on a form similar to that originally suggested by Durbin (e.g. Durbin (1995b)) produced the overall best agreement with stator vane heat transfer data. For the other model, with a reformulated more stable f wall boundary condition, a few different sets of model constants were found in the literature. The best results amongst these versions of the model were obtained with the constants used in Lien and Kalitzin (2001) or Cokljat et al. (2003).

Acknowledgements

Funding for the present work has been provided by STEM, Volvo Aero Corporation and ALSTOM Power via the Swedish Gas Turbine Center. Computer time provided by UNICC is gratefully acknowledged. The authors would also like to acknowledge Prof. K. A. Thole for supplying experimental data.

References

Cokljat, D., Kim, S., Iaccarino, G., Durbin, P., 2003. A comparative assessment of the $\overline{v^2}$–f model for recirculating flows. AIAA-2003-0765.

Davidson, L., Nielsen, P.V., Veningsson, A., 2003. Modifications of the v^2–f model for computing the flow in a 3D wall jet. In: Fourth International Symposium on Turbulence Heat and Mass Transfer. Antalya, Turkey.

Durbin, P., 1991. Near-wall turbulence closure modeling without 'damping functions'. Theoretical and Computational Fluid Dynamics 3, 1–13.

Durbin, P., 1995a. On the k-ε stagnation point anomaly. International Journal of Heat and Fluid Flow 17, 89–90.

Durbin, P., 1995b. Separated flow computations with the k–ε–v^2 model. AIAA Journal 33, 659–664.

Hermanson, K., Kern, S., Picker, G., Parneix, S., 2003. Predictions of external heat transfer for turbine vanes and blades with secondary flowfields. Journal of Turbomachinery 125, 107–113.

Iaccarino, G., 2001. Predictions of a turbulent separated flow using commercial CFD codes. Journal of Fluids Engineering 123, 819–828.

Kalitzin, G., 1999. Application of the $\overline{v^2}$–f model to aerospace configurations. Center for Turbulence Research Annual Research Briefs.

Kang, M., Thole, K., 2000. Flowfield measurements in the endwall region of a stator vane. Journal of Turbomachinery 122, 458–466.

Lien, F., Kalitzin, G., 2001. Computations of transonic flow with the $\overline{v^2}$–f turbulence model. International Journal of Heat and Fluid Flow 22, 53–61.

Lumley, J., 1978. Computational modeling of turbulent flows. Advances in Applied Mechanics 18, 123–176.

Manceau, R., Wang, M., Laurence, D., 2001. Inhomogeneity and isotropy effects on the redistribution term in Reynolds-Averaged Navier–Stokes modelling. Journal of Fluid Mechanics 438, 307–338.

Parneix, S., Durbin, P., Behnia, M., 1998. Computation of 3-D turbulent boundary layers using the $\overline{v^2}$–f model. Flow, Turbulence and Combustion 60, 19–46.

Radomsky, R., Thole, K., 2000. High free-stream turbulence effects on endwall heat transfer for a gas turbine stator vane. Journal of Turbomachinery 122, 699–708.

Sveningsson, A., 2003. Analysis of the performance of different $\overline{v^2}$–f turbulence models in a stator vane passage flow. Licentiate thesis. Department of Thermo and Fluid Dynamics, Chalmers University of Technology, Gothenburg, Sweden.

Sveningsson, A., Davidson, L., 2004. Computations of flow field and heat transfer in a stator vane passage using the $\overline{v^2}$–f turbulence model. In ASME Turbo Expo 2004 proceedings, Paper number GT2004-53586.